# Alteration profiles and impurity element distributions in magnetic fractions of weathered ilmenite

M. T. Frost, I. E. Grey,[1] I. R. Harrowfield, and C. Li

*CSIRO Division of Mineral Chemistry, P.O. Box 124*
*Port Melbourne 3207, Victoria, Australia*

## Abstract

Magnetic fractions of a commercial ilmenite concentrate from a near-surface deposit in Western Australia have been analyzed by quantitative X-ray diffraction and automated electron microprobe techniques. Phase distributions, composition histograms and variation of minor element concentrations (aluminium, silicon and manganese) have been determined with respect to the extent of alteration, as measured by the $Ti/(Ti + Fe)$ atomic ratio. The altered grains contain ilmenite/pseudorutile/rutile phase associations from alteration in groundwater, and ferrian ilmenite/rutile/H-239 (high temperature $Fe_2Ti_3O_9$) from surface alteration mechanisms. Grains from the different alteration environments were differentiated magnetically, with concentration of the products of surface alteration in the most-magnetic fractions.

Within each magnetic fraction the microprobe analyses show decreasing manganese and increasing aluminium and silicon concentrations with increasing $Ti/(Ti + Fe)$ atomic fraction. This confirms that during alteration, manganese is leached together with iron whereas aluminium and silicon are incorporated into the grains from the environment. Negative correlations occur between mean manganese and aluminium-silicon concentrations across the magnetic fractions. These are explained in terms of the different alteration mechanisms operating at depth and at the surface of the deposit.

## Introduction

We have recently reported an SEM and electron microprobe study of the distribution of the minor impurities, aluminium and silicon, in altered ilmenite grains from three Western Australian localities (Frost et al., 1983). The samples studied were commercial ilmenite concentrates derived from 90 ft. and 150 ft. strand lines at Capel, 150 km south of Perth, and from deposits at Eneabba, 200 km north of Perth. The 90 ft. strand Capel and Eneabba samples comprise mixtures of the phases ilmenite, pseudorutile and rutile, whereas the 150 ft. strand sample contains also the unusual assemblage (ferrian ilmenite)-(H-239)-rutile, where H-239 is a metastable phase with composition close to $Fe_2Ti_3O_9$. H-239 has been prepared by heating ilmenite or pseudorutile at temperatures below 800°C (Grey and Reid, 1972; Grey et al., 1973).

The results (Frost et al., 1983) represent analyses that were averaged over the various phase assemblages occurring in the bulk concentrates. In the present study an attempt has been made to more closely relate the impurity element distributions and alteration mechanisms to the individual phase types. The 150 ft. strand sample was split into a series of magnetic fractions, which were analyzed separately using electron microprobe and quantitative X-ray diffraction (XRD) techniques to determine

both the elements and phases present. The analysis for minor elements was extended to include manganese, in addition to aluminium and silicon.

## Experimental

### Material studied

The sample studied was a sulphate-grade commercial ilmenite concentrate derived from the 150 ft. strand line of the Yoganup Extended mine at Capel, W.A., which was supplied by Westralian Sands Ltd. The heavy mineral concentrate (HMC) was taken from the northern end of the strand line, where the deposit tapers upwards to a narrow, near-surface body. Some data were also obtained for comparison, on a concentrate from the 90 ft. strand line, which is a deep deposit lying mainly below the present water table. Magnetic fractions at 0.01, 0.05, 0.10, 0.20 and 0.30 and 0.40 A were obtained using a Cook isodynamic separator, with a side slope of 8° and a forward slope of 10°. The feed rate was about 50 g h$^{-1}$ and the magnetic fractions were recycled through the separator to ensure a clean separation.

### X-ray diffraction

Phases were identified in X-ray powder diffraction patterns, obtained with a Philips diffractometer fitted with a graphite monochromator and using $CuK\alpha$ radiation. A scan rate of 1° min$^{-1}$ was employed. When accurate lattice parameters were required, silicon was added as an internal standard.

Quantitative XRD analyses were performed using the Chung (1974) method, with Linde 1 $\mu$m corundum as internal standard. Samples for analysis were ground for 20 min in a McCrone mi-

---

Table 1.   Peak and background scan ranges for quantitative XRD

| Phase | | d-spacing | Scan range (2θ) Peak | Upper background | Lower background | ki* |
|-------|---|-----------|------|------------------|------------------|-----|
| Pseudorutile | -1 | 2.77 | 29.7-32.0 | 34.2-34.5 | 29.4-29.7 | 0.31 |
| + H-239 | -2 | 2.19 | 39.9-42.4 | 42.4-42.7 | 39.6-39.9 | 0.63 |
| Ilmenite | -1 | 2.75 | 32.0-34.2 | 34.2-34.5 | 29.4-29.7 | 2.09 |
|  | -2 | 1.87 | 47.8-50.0 | 50.0-50.3 | 47.5-47.8 | 0.68 |
| Rutile |  | 3.25 | 26.9-28.5 | 28.5-28.8 | - | 2.75 |
| Corundum |  | 2.08 | 42.7-45.0 | 45.0-45.3 | 42.4-42.7 |  |

*ki = reference intensity ratio (Chung, 1974).

Table 2.   Quantitative XRD analyses of magnetic fractions of ilmenite concentrates

| Magnetic fraction | wt.% | Rutile | Ilmenite | Pseudorutile/ H-239 | Total |
|-------------------|------|--------|----------|---------------------|-------|
| **150 ft strand** | | | | | |
| 0.01 A | 6.3 | 21.4 | 50.8 | 22.0 | 94.2 |
| 0.05 | 17.3 | 18.1 | 42.1 | 29.6 | 89.8 |
| 1.10 | 23.6 | 14.3 | 45.0 | 34.7 | 94.0 |
| 0.20 | 44.0 | 7.9 | 57.0 | 33.3 | 98.2 |
| 0.30 | 7.2 | 8.6 | 35.8 | 57.1 | 101.5 |
| 0.40 | 0.9 | 20.0 | 11.6 | 59.9 | 91.5 |
| Non mags. | 0.7 | * | | | |
| **90 ft strand** | | | | | |
| 0.01 Amps | 0.3 | * | | | |
| 0.05 | 1.8 | * | | | |
| 0.10 | 16.5 | 3.0 | 37.3 | 53.8 | 94.1 |
| 0.20 | 43.4 | 2.8 | 40.0 | 54.2 | 97.0 |
| 0.30 | 33.3 | 2.6 | 21.0 | 72.6 | 96.2 |
| 0.40 | 3.7 | * | | | |
| Non mags. | 1.0 | * | | | |

*Insufficient material for analysis.

cronizing mill and then mixed with corundum in the weight ratio 60:40, in a SPEX vibrating mill. Integrated peak intensities were obtained by a microprocessor-controlled step-scan procedure. Stepping intervals of 0.01° 2θ were used with 1 second counts per step, accumulating typically 7000 to 30000 counts per scan interval. The peak and background scan ranges used, together with the reference intensity ratios, ki, are given in Table 1.

Reference standards used for XRD were natural rutile from Capel, W.A., massive unaltered ilmenite from China, pure pseudorutile from Neptune Island, South Australia (Larrett and Spencer, 1971), and synthetic H-239 prepared by oxidizing synthetic ilmenite at 770°C (Grey and Reid, 1972; Rao and Rigaud, 1974). Care was taken in selecting standards with similar crystallite sizes (as determined from XRD peak broadening) to the phases in the altered ilmenite grains.

The scan ranges given in Table 1 were carefully selected to avoid interference from peaks due to minor impurity phases such as quartz, goethite and anatase. For ilmenite, pseudorutile and H-239, independent estimates were obtained from two different peaks. Where H-239 and pseudorutile occurred in the same sample, the individual contributions could not be resolved and the common peak at 2θ ~41° was found to give the most reliable estimate of the combined ferric titanates (after contributions from rutile and ilmenite had been estimated and subtracted). The precision and accuracy of the procedure was tested on synthetic mixtures of the reference standards. The mean weight percents and standard deviations for five determinations on the synthetic mixture Ilmenite$_{30}$Pseudorutile$_{50}$Rutile$_{20}$ were ilmenite, 31.5(1.4), pseudorutile, 48.1(2.8) and rutile 20.8(0.6).

*Microprobe analyses*

The automated analytical procedure, described in detail by Frost et al. (1983), differs mainly with the analysis of the additional element Mn. The analyses were performed at 20 kV and 30 nA using the same fully automated Jeol JXA50A microprobe. The procedure involves step-scanning across samples automatically, passing along parallel lines, 4200 μm long and 200 μm apart. Grains of interest were distinguished from plastic or from impurities by the Ti and/or Al count rates exceeding 500 cps during a 1/32 second counting time. By reducing the step length to 3 μm, well below the normal distance that separates grains, it was possible to define each grain separately. The inclusion of Al in the grain selection test allowed analytical data to be obtained on clay coatings and inclusions. One in ten of points showing high Ti and/or Al was analysed for Fe, Ti, Al, and Mn, counting for 4 seconds on each element. In this way, complete analyses were performed every 30 μm. Measured concentrations were cor-

rected using the Mk7ZAF program (Frost, 1977) and the grain number and corrected concentrations were filed.

## Results and discussion

*Magnetic separation and XRD analyses*

The weight percents of material in the different magnetic fractions, together with the phase analysis of each fraction, from quantitative XRD, are given in Table 2. An unusual feature of the magnetic separation results is the relatively high levels of strongly magnetic material, with almost one quarter of the 150 ft. strand ilmenite concentrate reporting to the combined 0.01 and 0.05 A fractions. For comparison, ilmenite concentrates from the 90 ft. strand line and other deposits near Capel have less than 3 wt.% in the 0.01 and 0.05 A magnetic fractions (Table 2). XRD patterns for the fractions separated at the two lowest current settings showed appreciable shifts in the positions of the ilmenite diffraction lines to higher angles, corresponding to formation of hematite-ilmenite solid solutions. The presence of ferrian-ilmenite in the higher magnetic fractions of ilmenite concentrates from the Capel region was recently confirmed by Wort and Jones (1981), using XRD methods on magnetically aligned samples. Least squares refinement of the 2θ values for the ilmenite peaks in the XRD patterns for the 0.01 and 0.20 A magnetic fractions gives hexagonal lattice parameters, $a = 5.079(1)$, $c = 13.937(9)$ Å and $a = 5.080(1)$, $c = 14.047(9)$ Å respectively. For comparison, lattice parameters were determined for fresh ilmenite from a biotite-quartz-feldspar gneiss, giving $a = 5.080(1)$, $c = 14.044(5)$ Å. The gneiss was collected from the nearby Archean metamorphic and igneous complex in the Leeuwin-Naturaliste ridge, considered to be the provenance of the heavy mineral deposits (Baxter, 1977). Microprobe analysis of the fresh ilmenite gave the composition $Fe_{1.04}Mn_{0.01}Ti_{0.95}O_3$. The parameters for ilmenite from the 0.20 A fraction are the same as those for the source ilmenite, whereas $c$ for ilmenite from the 0.01 A fraction is considerably smaller.
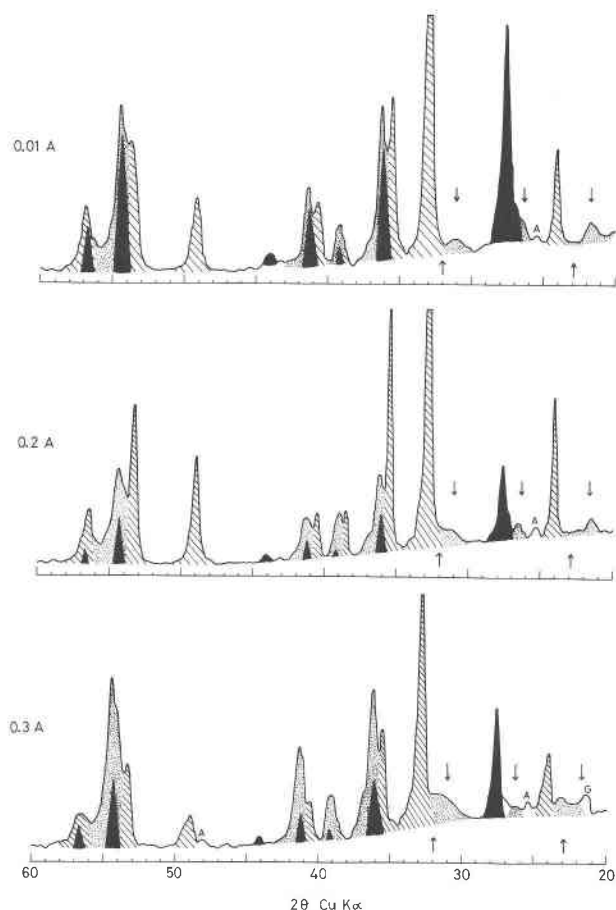
Fig. 1. XRD powder patterns of magnetic fractions of the 150 ft. strand ilmenite concentrate. Black shading is rutile, cross-hatched shading is ilmenite and dotted shading is pseudorutile and H-239. The upper row of arrows indicate H-239, and the lower arrows indicate pseudorutile peak positions. A = anatase, G = goethite.

Using the lattice parameter-composition curve reported by Lindsley (1965) the ilmenite composition in the 0.01 A fraction is $(Fe_2O_3)_{0.30}(FeTiO_3)_{0.70}$ (estimated).

The quantitative XRD results for the 150 ft. strand material appear anomalous, in that the most magnetic fractions contain the highest levels of the *non*-magnetic phase rutile, as shown in Table 2 and Figure 1. With decreasing magnet current from 0.2 to 0.01 A, the rutile content increases by about 300%. This unusual observation may be explained by postulating a fine-scale intergrowth of rutile in strongly magnetic ferrian-ilmenite. Such an association is known to result from intermediate-temperature (~700°C) oxidation roasting of ilmenite (Haggerty, 1976) according to the equation:

$$(1 + x)FeTiO_3 \xrightarrow{\text{oxidation}} (FeTiO_3)_{1-x}(Fe_2O_3)_x + 2xTiO_2 \quad (1)$$
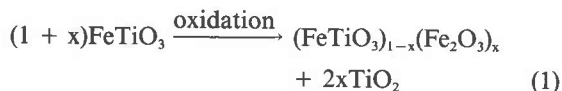
Further evidence that ilmenite from the 150 ft. strand has undergone elevated temperature oxidation is the presence

of H-239, which is concentrated in the 0.01–0.20 A magnetic fractions (Fig. 1). In progressively weaker magnetic fractions, the XRD lines due to H-239 are replaced by those of pseudorutile.

In contrast to the results for the 150 ft. strand, ilmenite concentrates from the 90 ft. strand show very low levels of ferrian ilmenite and H-239. The rutile contents of individual magnetic fractions are also much lower (Table 2). These differences may be explained in terms of the different weathering environments for the two heavy mineral deposits, and will be discussed below.

The quantitative XRD data given in Table 2 show that ilmenite is concentrated in the 0.01–0.20 A fractions, pseudorutile is concentrated in the 0.30 and 0.40 A fractions and rutile is concentrated at both ends of the range and is at a minimum in the 0.20 A fraction. The results for material separated at 0.01–0.1 A may be interpreted as due to magnetic fractionation of ferrian-ilmenite according to the composition and amount of ilmenite-hematite solid solution, as originally proposed by Wort and Jones (1980). For grains separated in the range 0.2–0.4 A, the decrease in magnetic properties is due to increasing extent of alteration of ilmenite to weakly magnetic pseudorutile and non-magnetic rutile.

The results for the 150 ft. strand concentrate differ from those reported for altered Capel ilmenite by Wort and Jones (1980, 1981) in two respects: the amorphous content of the altered grains and the levels of rutile in the strongly magnetic fractions. The amorphous content is obtained by subtracting the sum of the crystalline phases from 100%. Wort and Jones (1980) reported amorphous contents as high as 41% for the 0.05 A fraction whereas the results given in Table 2 deviate from 100% by only 5–10% and at least some of this discrepancy is due to minor crystalline phases not analysed for, such as anatase, quartz and goethite. Whereas Wort and Jones (1980) used synthetic ilmenite and rutile as reference standards, we used natural samples with crystallite sizes comparable with those of the phases analysed. The amorphous content has thus been incorporated in our analytical results for the poorly crystalline alteration products. The rutile contents (3–4 wt.%) reported by Wort and Jones (1980, 1981) are much lower than the values obtained here for the 150 ft. strand concentrate but are comparable with the rutile contents in the 90 ft. strand material, Table 2. This suggests that the material studied by Wort and Jones (1980) was derived from a deep-lying deposit, similar to the 90 ft. strand deposit, where surface reactions to form rutile are unlikely to occur to any great extent.

In addition to the powder XRD studies summarized in Table 2, we carried out single-crystal XRD studies on individual grains excavated from the polished sections used for the microprobe analyses. X-ray precession photographs for excavated grains confirmed the presence of H-239, Figure 2. This phase gave single-crystal diffraction patterns that could be indexed using the cell parameters previously reported for $Fe_2Ti_3O_9$ (Grey et al., 1973). The single-grain XRD studies showed the presence of rutile,
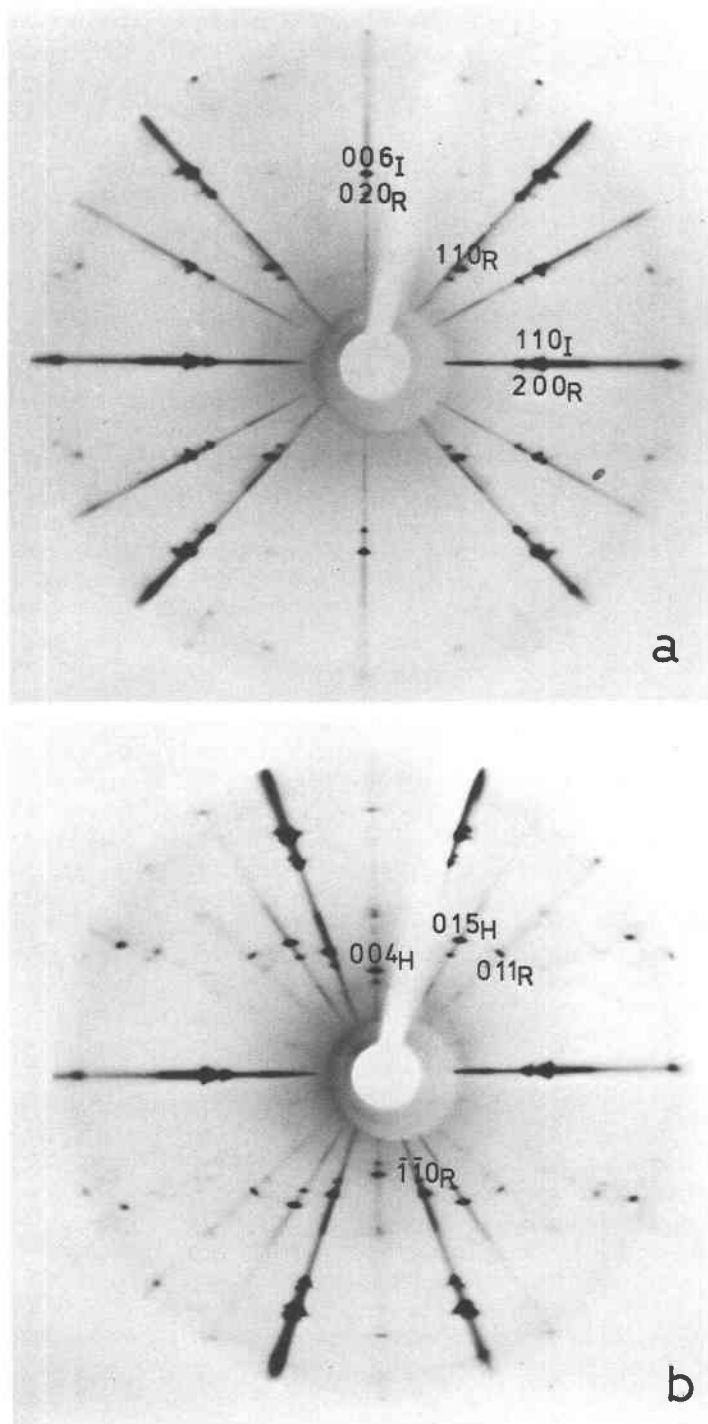
Fig. 2. Precession photographs of a grain from the 0.05 A magnetic fraction, Ti/(Ti + Fe) = 0.59, comprising oriented crystals of ilmenite (I), rutile (R) and H-239 (H). (a) [1$\bar{1}$0] zone axis pattern for ilmenite, together with [001] zone axis pattern for rutile. (b) [100] zone axis pattern for H-239, together with [$\bar{1}$1$\bar{1}$] zone axis pattern for rutile (twinned).

in oriented intergrowth with ilmenite, Figure 2(a), in grains with compositions spanning the full range of Ti(Ti + Fe) ratios. This is in contrast to our previous single-grain studies on Eneabba ilmenite concentrate (Frost et al., 1983) that showed rutile was restricted to grains with Ti/(Ti + Fe) > 0.7. The rutile-ilmenite associations in the 150 ft. strand concentrate derive from oxidation-roast reactions as given by equation (1) and also by supergene alteration

Table 3. Sample of output data from automated microprobe scan

```
Range of function 0.7400 to 0.7700
No analysis included if total is found below 0.8000
Data are expressed as oxides
```

| Line | Grain | Fe | Mn | Ti | Si | Al | Total | Ti/(Ti+Fe) |
|------|-------|------|------|------|------|------|-------|------------|
| 1 | 2 | 0.2436 | 0.0038 | 0.7130 | 0.0016 | 0.0113 | 0.9735 | 0.7452 |
| 1 | 2 | 0.2353 | 0.0033 | 0.7238 | 0.0025 | 0.0112 | 0.9763 | 0.7545 |
| 1 | 2 | 0.2315 | 0.0028 | 0.7318 | 0.0017 | 0.0168 | 0.9847 | 0.7595 |
| 2 | 2 | 0.2203 | 0.0061 | 0.6718 | 0.0016 | 0.0143 | 0.9143 | 0.7529 |
| 2 | 12 | 0.2107 | 0.0016 | 0.6070 | 0.0015 | 0.0096 | 0.8306 | 0.7422 |
| 3 | 1 | 0.2344 | 0.0013 | 0.6890 | 0.0022 | 0.0285 | 0.9555 | 0.7460 |
| 3 | 27 | 0.2261 | 0.0028 | 0.6976 | 0.0005 | 0.0150 | 0.9423 | 0.7551 |
| 3 | 27 | 0.2325 | 0.0029 | 0.6851 | 0.0012 | 0.0147 | 0.9365 | 0.7464 |
| 3 | 27 | 0.2337 | 0.0021 | 0.6945 | 0.0006 | 0.0147 | 0.9459 | 0.7480 |
| 3 | 27 | 0.2385 | 0.0015 | 0.6999 | 0.0006 | 0.0155 | 0.9561 | 0.7457 |
| 3 | 35 | 0.0911 | 0.0007 | 0.2963 | 0.0041 | 0.0173 | 0.4098 | 0.7647 |
| 5 | 23 | 0.2320 | 0.0011 | 0.7417 | 0.0004 | 0.0144 | 0.9897 | 0.7616 |
| 6 | 4 | 0.1915 | 0.0004 | 0.6326 | 0.0025 | 0.0116 | 0.8387 | 0.7675 |
| 6 | 4 | 0.2153 | 0.0032 | 0.6313 | 0.0018 | 0.0111 | 0.8629 | 0.7455 |
| 6 | 6 | 0.2042 | 0.0032 | 0.6455 | 0.0030 | 0.0174 | 0.8734 | 0.7595 |
| 6 | 21 | 0.1876 | 0.0054 | 0.5599 | 0.0069 | 0.0302 | 0.7901 | 0.7489 |
| 6 | 38 | 0.2390 | 0.0006 | 0.7231 | 0.0004 | 0.0147 | 0.9781 | 0.7514 |
| 6 | 38 | 0.2245 | 0.0002 | 0.7358 | 0.0005 | 0.0151 | 0.9763 | 0.7660 |
| 6 | 38 | 0.2389 | 0.0011 | 0.7217 | 0.0008 | 0.0168 | 0.9794 | 0.7511 |
| 7 | 16 | 0.2283 | 0.0002 | 0.7057 | 0.0021 | 0.0240 | 0.9604 | 0.7555 |
| 7 | 25 | 0.2377 | 0.0034 | 0.6819 | 0.0010 | 0.0109 | 0.9350 | 0.7414 |
| 8 | 21 | 0.2340 | 0.0000 | 0.7068 | 0.0037 | 0.0213 | 0.9660 | 0.7511 |
| 9 | 14 | 0.2116 | 0.0000 | 0.6889 | 0.0027 | 0.0151 | 0.9183 | 0.7649 |
| 9 | 14 | 0.2243 | 0.0024 | 0.6748 | 0.0018 | 0.0146 | 0.9181 | 0.7503 |
| 9 | 14 | 0.2213 | 0.0017 | 0.6982 | 0.0019 | 0.0163 | 0.9395 | 0.7592 |
| 9 | 14 | 0.2397 | 0.0009 | 0.6892 | 0.0015 | 0.0181 | 0.9496 | 0.7418 |

```
Element Fe -
No. of points in range       24 mean concentration 0.2270      Std. Dev. 0.0130

Element Mn -
No. of points in range       "   "         "         0.0019      "    "     0.0015

Element Ti -
No. of points in range       "   "         "         0.6913      "    "     0.0351

Element Si -
No. of points in range       "   "         "         0.0016      "    "     0.0009

Element Al -
No. of points in range       "   "         "         0.0155      "    "     0.0043
```

Table 4. Mean microprobe elemental analysis (wt.%) from three independent scans for the 0.05 A magnetic fraction

| | Scan 1 | Scan 2 | Scan 3 | Weighted average |
|------|--------|--------|--------|------------------|
| No. of points analysed | 567 | 491 | 742 | |
| $Fe_2O_3$ | 37.6 | 35.9 | 37.3 | 37.0(0.9) |
| $TiO_2$ | 51.3 | 52.9 | 53.8 | 52.8(1.3) |
| MnO | 0.90 | 1.17 | 1.07 | 1.04(0.14) |
| $Al_2O_3$ | 0.77 | 0.74 | 0.81 | 0.78(0.04) |
| $SiO_2$ | - | 0.13 | 0.10 | 0.11(0.02) |
| Total | 90.6 | 90.8 | 93.1 | 91.7 |
| Ti/(Ti + Fe) | 0.58 | 0.60 | 0.59 | 0.59 |

## Electron microprobe analyses

Automated microprobe scans were carried out on the six magnetic fractions of the 150 ft. strand concentrate. Approximately 10 line scans were made for each specimen, each involving about 100 point analyses from about 30 separate grains. Thus a total of more than 6000 analyses from about 1800 grains have been made, ensuring that the results are representative of the bulk material.

A typical example of processed data for one of the samples is shown in Table 3. The data are grouped according to the Ti/(Ti + Fe) atomic ratio. The output lists the weight fractions of $Fe_2O_3$, $TiO_2$, MnO, $SiO_2$ and $Al_2O_3$ for each point analysis, as well as the analysis total and Ti/(Ti + Fe) ratio. Each analysis is identified by giving the scan line number and grain number. During the line scans, the electron beam burns a fine line in the polished-section surface that is visible using an optical microscope, thus aiding the location of individual grains for excavation and further characterization by single-crystal XRD.

At the end of each group of analyses the average weight

of ilmenite and ferrian ilmenite directly to rutile (Rumble, 1976). We have previously noted the prevalence of grains comprising relatively unaltered ilmenite cores surrounded by rims of leucoxene in the 150 ft. strand bulk concentrate (Frost et al., 1983).

Table 5. Summary of electron microprobe analytical data

| | Data | | Magnetic fraction separated at (A): | | | | | |
|---|------|---------|---------------|--------------|--------------|--------------|--------------|--------------|
| | | | 0.01 | 0.05 | 0.10 | 0.20 | 0.30 | 0.40 |
| | No. of grains analysed | | 960 | 1800 | 860 | 1005 | 970 | 921 |
| $Fe_2O_3$ | - | minimum | 2.4 | 5.0 | 3.6 | 2.4 | 5.8 | 0.84 |
| | - | maximum | 57.5 (13.0)* | 57.5 (11.1) | 56.7 (13.5) | 57.2 (19.3) | 53.0 (15.8) | 52.5 (2.7) |
| | - | mean | 39.4 (26.9) | 37.0 (26.8) | 41.1 (25.2) | 40.6 (21.7) | 36.9 (23.9) | 30.3 (23.9) |
| $TiO_2$ | - | minimum | 0.38 | 1.0 | 0.60 | 30.7 | 39.5 | 0.92 |
| | - | maximum | 80.7 | 83.3 | 83.9 | 92.7 | 80.5 | 95.9 |
| | - | mean | 54.6 (56.5) | 52.8 (57.9) | 53.9 (57.1) | 55.3 (55.4) | 56.9 (56.9) | 63.2 (61.1) |
| MnO | - | minimum | 0 | 0 | 0 | 0 | 0 | 0 |
| | - | maximum | 3.1 | 4.2 | 3.9 | 7.0 | 8.8 | 14.8 |
| | - | mean | 0.72 (1.2) | 1.0 (1.3) | 0.93 (1.4) | 1.3 (1.5) | 1.5 (1.6) | 0.83 (-) |
| $Al_2O_3$ | - | minimum | 0.08 | 0.20 | 0.05 | 0.05 | 0.13 | 0.19 |
| | - | maximum | 46.7 | 52.6 | 56.7 | 8.8 | 6.0 | 53.9 |
| | - | mean | 0.84 (1.4) | 0.78 (1.4) | 0.68 (1.3) | 0.45 (0.96) | 0.48 (1.0) | 0.90 (-) |
| $SiO_2$ | - | minimum | 0 | 0 | 0 | 0.00 | 0.00 | 0.00 |
| | - | maximum | 46.7 | 19.6 | 39.9 | 4.3 | 14.2 | 20.7 |
| | - | mean | 0.19 (0.42) | 0.11 (0.40) | 0.14 (0.44) | 0.09 (0.29) | 0.14 (0.42) | 0.27 (-) |
| Ti/(Ti + Fe) | | | 0.58 | 0.59 | 0.57 | 0.57 | 0.61 | 0.68 |
| Mean analysis total | | | 95.7 | 92.2 | 96.8 | 97.7 | 95.9 | 95.3 |

*Figures given in parentheses are from chemical analyses, supplied by W.S.L. The two numbers given in the $Fe_2O_3$-row are FeO and $Fe_2O_3$ respectively, and their sum must be used in comparing with the microprobe results.
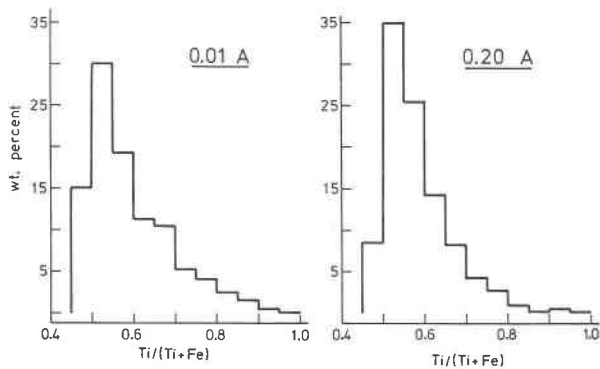
Fig. 3. Composition histograms for the 0.01 A and 0.20 A magnetic fractions.

percents of oxides and their standard deviations for that particular Ti/(Ti + Fe) range are listed. Data with low totals (a value of 80% was chosen for the cutoff) were not used in the statistical analysis. Low totals result from analyses near the edges of grains or from analyses of porous grains.

For each magnetic fraction the individual group analyses have been combined to give the average weight percents of oxides. For the 0.05 A magnetic fraction, three independent data collections were made and the results analysed to obtain an estimate of the precision of the method. The results for the three scans are given in Table 4. The weighted average analyses over the three data sets have been determined and the associated standard deviations are given in parentheses.

A summary of the statistical analysis of the full data set is given in Table 5. The average analyses shown were calculated for the Ti/(Ti + Fe) range 0.45–1.00. Analyses with lower ratios than 0.45 were observed to correspond mainly to high-silicon, aluminium-containing phases that were present as clay coatings, and inclusions. The maximum and minimum analyses for each element are also given. The $TiO_2$ contents are particularly variable, from values close to zero in the clay coatings and inclusions, to values in the range 80–96% in the highly altered leucoxene phases. There is little variation in the mean $Fe_2O_3$ or $TiO_2$ contents over the four most-magnetic fractions, 0.01–0.2 A. From the 0.2 to 0.4 A fractions, the $TiO_2$ content increases and the $Fe_2O_3$ content decreases, consistent with the results reported by Wort and Jones (1980, 1981).

The mean values of the microprobe analyses are compared with values obtained from wet-chemical analyses, given in parentheses in Table 5. There is reasonable agreement for the major elements iron and titanium, the mean difference being 3.3 wt.% for both elements. The $Al_2O_3$ and $SiO_2$ analyses from the microprobe scans are lower than the bulk chemical analysis figures by factors of 2 and 3, respectively; the difference may be explained by high-Al,Si clay coatings and inclusions, with Ti/(Ti + Fe) < 0.45, which were not included in the statistical analysis. The wet-chemical and microprobe analyses for these minor elements both show the same trends of maximum concentration at either end of the magnetic susceptibility range, with minima in the 0.20 A magnetic fraction. This fraction contains the highest fresh ilmenite content, as evidenced by the FeO contents in Table 5. The third minor element, manganese, shows an inverse correlation with

Table 6. Alteration profiles and impurity element distributions in individual magnetic fractions

| Ti/(Ti + Fe) range | wt.% | $Al_2O_3$ | $SiO_2$ | MnO | wt.% | $Al_2O_3$ | $SiO_2$ | MnO | wt.% | $Al_2O_3$ | $SiO_2$ | MnO |
|---|---|---|---|---|---|---|---|---|---|---|---|---|
| | 0.01 A fraction | | | | 0.05 A fraction | | | | 0.10 A fraction | | | |
| 0.45–0.50 | 15.1 | 0.42 | 0.04 | 0.84 | 8.6 | 0.30 | 0 | 1.06 | 21.5 | 0.28 | 0.03 | 0.88 |
| 0.50–0.55 | 30.1 | 0.51 | 0.07 | 0.91 | 26.0 | 0.37 | 0.04 | 1.32 | 25.6 | 0.38 | 0.07 | 1.13 |
| 0.55–0.60 | 19.2 | 0.83 | 0.16 | 0.94 | 26.4 | 0.58 | 0.10 | 1.30 | 21.7 | 0.56 | 0.13 | 1.15 |
| 0.60–0.65 | 11.3 | 1.13 | 0.28 | 0.64 | 16.5 | 0.88 | 0.16 | 1.22 | 15.5 | 0.97 | 0.21 | 0.89 |
| 0.65–0.70 | 10.4 | 1.37 | 0.35 | 0.46 | 10.4 | 1.20 | 0.22 | 0.82 | 7.3 | 1.37 | 0.31 | 0.52 |
| 0.70–0.75 | 5.2 | 1.54 | 0.37 | 0.35 | 5.2 | 1.47 | 0.26 | 0.58 | 3.1 | 1.73 | 0.38 | 0.40 |
| 0.75–0.80 | 4.1 | 1.77 | 0.49 | 0.24 | 2.9 | 1.75 | 0.33 | 0.38 | 2.3 | 1.78 | 0.38 | 0.31 |
| 0.80–0.85 | 2.5 | 2.04 | 0.73 | 0.20 | 1.8 | 2.30 | 0.37 | 0.18 | 1.5 | 2.28 | 0.48 | 0.12 |
| 0.85–0.90 | 1.6 | 1.84 | 0.58 | 0.07 | 1.7 | 1.92 | 0.36 | 0.10 | 0.6 | 2.51 | 0.49 | 0.04 |
| 0.90–0.95 | 0.4 | 1.23 | 0.32 | 0 | 0.3 | 0.84 | 0.35 | 0.02 | 0.7 | 2.14 | 0.32 | 0.02 |
| 0.95–1.00 | 0.1 | 0.54 | 0.30 | 0 | 0.1 | – | – | – | 0.1 | 0.31 | 0 | 0 |
| | 0.20 A fraction | | | | 0.30 A fraction | | | | 0.40 A fraction | | | |
| 0.45–0.50 | 8.5 | 0.21 | 0.02 | 1.04 | 1.2 | 0.25 | 0.01 | 1.15 | 0 | – | – | – |
| 0.50–0.55 | 34.9 | 0.25 | 0.04 | 1.34 | 18.5 | 0.34 | 0.04 | 1.49 | 1.6 | 0.33 | 0.01 | 0.90 |
| 0.55–0.60 | 25.4 | 0.37 | 0.06 | 1.52 | 29.5 | 0.38 | 0.08 | 1.69 | 8.8 | 0.53 | 0.13 | 0.97 |
| 0.60–0.65 | 14.2 | 0.54 | 0.16 | 1.47 | 26.5 | 0.45 | 0.12 | 1.86 | 31.9 | 0.60 | 0.17 | 1.09 |
| 0.65–0.70 | 8.2 | 0.81 | 0.24 | 0.90 | 13.8 | 0.65 | 0.30 | 1.25 | 29.6 | 0.76 | 0.25 | 1.12 |
| 0.70–0.75 | 4.2 | 1.03 | 0.19 | 0.44 | 5.2 | 0.82 | 0.40 | 0.90 | 9.8 | 1.05 | 0.33 | 0.74 |
| 0.75–0.80 | 2.7 | 1.48 | 0.19 | 0.22 | 3.0 | 0.94 | 0.32 | 0.28 | 7.9 | 1.34 | 0.41 | 0.36 |
| 0.80–0.85 | 0.9 | 1.64 | 0.38 | 0.29 | 1.1 | 1.37 | 0.50 | 0.17 | 5.3 | 1.46 | 0.50 | 0.25 |
| 0.85–0.90 | 0.2 | 1.23 | 0.56 | 0.15 | 1.0 | 1.17 | 0.40 | 0.07 | 3.2 | 1.64 | 0.73 | 0.22 |
| 0.90–0.95 | 0.6 | 0.98 | 0.46 | 0.20 | 0.2 | 0.98 | 0.41 | 0 | 1.1 | 1.68 | 0.89 | 0.07 |
| 0.95–1.00 | 0.1 | – | – | – | – | – | – | – | 0.8 | 0.98 | 0.66 | 0.12 |
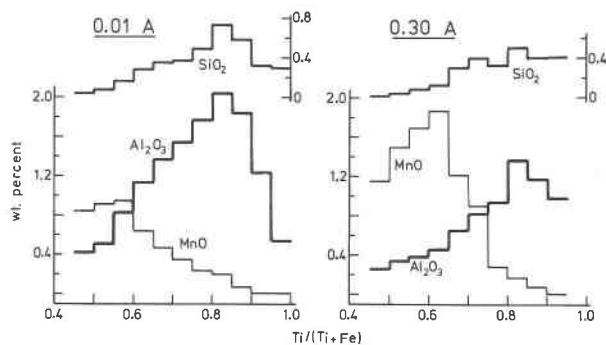
Fig. 4. Minor element distributions for the 0.01 A and 0.30 A magnetic fractions.

the highest concentrations in the 0.20 and 0.30 A fractions, and minima at either end.

*Composition histograms*

The composition distributions in the magnetic fractions are given in Table 6, as the frequency of occurrence of phases having Ti/(Ti + Fe) ranging from 0.45 to 1.00 in increments of 0.05. As discussed by Frost et al. (1983), this is a close approximation to the weight fraction of the phases in each Ti/(Ti + Fe) range for random distributions in the exposed grains of polished sections.

The histograms for the four most-magnetic fractions, 0.01 to 0.20 A, are all very similar, with maxima in the Ti/(Ti + Fe) range 0.5–0.55, that is, compositions close to that of ilmenite (Fig. 3). In the 0.30 and 0.40 A magnetic fractions, the progressive shift of the histogram peak to higher Ti/(Ti + Fe) ratios reflects the increasing extent of alteration of ilmenite to pseudorutile and rutile.

The conversion of ilmenite to a mixture of ferrian-ilmenite plus rutile in the most-magnetic fractions is not manifested by the expected bimodal distribution in the composition histograms, indicating that intergrowth of these phases occurs on a finer scale than can be resolved by the electron beam ($\sim 5 \mu m$). This is consistent with the oxidation reaction (1) (and formation of H-239) being a secondary alteration phenomenon that produces no significant phase growth or change in bulk composition.

*Minor element distributions*

The mean weight percents of the oxides of manganese, aluminium and silicon in each 0.05 increment of the Ti/(Ti + Fe) ratio are given in Table 6. The minor element distribution patterns show the same general trends for all six magnetic fractions. With increasing Ti/(Ti + Fe) ratio the minor element concentrations initially increase, then pass through a maximum, and decrease with further iron removal. The positions of the maxima are quite different for manganese and for aluminium-silicon, being within the Ti/(Ti + Fe) range 0.6–0.7 for the former and 0.8–0.9 for the latter elements. In the Ti/(Ti + Fe) range $\sim 0.6$–0.9 there is negative correlation between manganese and aluminium-silicon concentrations, Figure 4. The distribu-

tion curves for aluminium-silicon agree generally with our previously reported results for a bulk specimen of the 150 ft. strand concentrate (Frost et al., 1983). However, due to the smaller number of grains analysed in the previous study, the decrease in Al,Si concentrations at high Ti/(Ti + Fe) ratios was not detected.

Important differences in detail of the distribution curves occur between the different magnetic fractions as shown by a comparison of the curves for the 0.01 and 0.30 A magnetic fractions (Fig. 4). These differences will be discussed in relation to the different alteration phases in the following section.

*Interpretation of results in terms of alteration mechanisms*

The 150 ft. strand ilmenite concentrate studied here was obtained from a bulk HMC produced from the large-scale mining of a face extending from the surface to some meters below the water table. In the plant processing of the HMC, alteration phase assemblages from both groundwater and surface environments have been mixed together. The results presented in the previous sections show that the laboratory magnetic separation has segregated the alteration products from the two weathering environments. We will first summarize the different alteration mechanisms operating at depth and at the surface of the deposit, and then apply the models to interpret the composition variations in the different magnetic fractions.

In a groundwater environment, ilmenite alters to pseudorutile by oxidation of all the ferrous iron to ferric, together with diffusion of one-third of the ferric ions out of the otherwise unchanged anion lattice. Alteration to pseudorutile and accompanying reactions have been discussed in detail by several authors (Temple, 1966; Grey and Reid, 1975; Dimanche and Bartholomé, 1976). Hydration also plays an important role in the alteration of ilmenite in groundwater (Flinter, 1959; Gevorkyan and Tananayev, 1964). Recent studies on pseudorutile (Grey et al., 1983) show that pseudorutile is an oxyhydroxide mineral, with an extended range of homogeneity due to proton exchange for iron (Frost et al., 1983).

Alteration of ilmenite beyond the pseudorutile composition limit (Ti/(Ti + Fe) $\simeq 0.7$) involves removal of oxygen also, leading to the formation of rutile or anatase (Grey and Reid, 1975; Anand and Gilkes, 1985). This proceeds by an incongruent leaching mechanism in mildly reducing acidic solutions. The iron titanate dissolves and iron stays in solution whereas the titanium reprecipitates back on the original grains as a colloidal hydrated oxide that crystallizes as rutile or anatase. The conditions required for this type of alteration are met in the near-surface zones of the deposit where leaching agents occur, such as humic acid and sulphuric acid, derived from decomposition of vegetation and from rain, respectively (Lynd, 1960).

Direct leaching of ilmenite by soil acids also occurs in the near-surface zones of HMC deposits. Ferrian-ilmenite is particularly susceptible to strong alteration of this type

(Rumble, 1976). A scanning electron microscope study of grains from the 150 ft. strand concentrate showed relatively unaltered ilmenite cores rimmed with leucoxene due to this type of alteration (Frost et al., 1983).

Finally, dry oxidation of ilmenite at elevated temperatures can produce mixtures of ferrian ilmenite plus rutile, according to equation (1), and H-239, $Fe_2Ti_3O_9$. In the laboratory these reactions require temperatures above a few hundred degrees. Lynd (1960) suggests that surface sands exposed to the sun in warm climates may be heated to temperatures of 45–50°C and this may be adequate to produce the above oxidation products over thousands of years. Alternatively, these products could form locally, around burning logs and root systems during bushfires and then be dispersed throughout the upper layer of the deposit by normal soil homogenization mechanisms. We have confirmed that ferrian-ilmenite-rutile-H-239 assemblages are confined to the near-surface region of HMC deposits from a study of drill-core samples taken at different depths in the 215 ft. strand line at the Yoganup extended deposit (I. E. Grey, unpublished data).

The 90 ft. strand deposit lies many meters below the present water table, and the results presented for ilmenite concentrate from this deposit (Table 2) confirm that alteration to pseudorutile is the dominant process operating in this deposit. In contrast, the 150 ft. strand concentrate contains phase assemblages from both groundwater and surface alterations. Ferrian ilmenite-rutile and H-239 from elevated temperature oxidation and ferrian ilmenite-rutile from incongruent leaching are concentrated in the most-magnetic fractions, 0.01–0.1 A; relatively unaltered ilmenite is dominant in the 0.2 A fraction and pseudorutile from groundwater alteration is concentrated in the 0.3 and 0.4 A fractions. Rutile derived from leaching of pseudorutile also resides in the 0.4 A fraction.

Minor element distributions as a function of Ti/(Ti + Fe) are compared in Figure 4 for magnetic fractions containing predominantly products from surface alteration (0.01 A) and groundwater alteration (0.3 A). We will describe first the simpler case of the 0.3 A fraction, involving alteration of ilmenite to pseudorutile (stage 1), together with some further alteration of pseudorutile to rutile (stage 2).

The distribution curve for manganese shows that in the first stage of alteration, manganese is not removed with the iron but is enriched in the iron-depleted ferric titanate. This may be explained by the relative oxidation potentials of $Mn^{2+}/Mn^{3+}$ and $Fe^{2+}/Fe^{3+}$. While iron is being oxidized to the ferric state, the manganese remains as $Mn^{2+}$, which is too large to diffuse out of the lattice. In the second stage of alteration, involving leaching of pseudorutile, the manganese goes into solution along with iron, while the titanium reprecipitates on the host grain. Where this mixing of reprecipitated titanium oxide and unattacked pseudorutile occurs on a fine scale compared with the area the electron beam analyses, the resultant analyses will show a negative correlation between the Mn content and Ti/(Ti + Fe) for ratios greater than ~0.7, as observed.

Aluminium and silicon are also enriched due to iron depletion during the first stage of alteration, but their concentrations remain quite low, $Al_2O_3 \leq 0.4\%$ and $SiO_2 \leq 0.1\%$. For Ti/(Ti + Fe) > 0.7, corresponding to the second stage of alteration, the aluminium and silicon levels increase rapidly with increasing Ti/(Ti + Fe) ratios, to maximum mean values near 1.5% $Al_2O_3$ and 0.5% $SiO_2$. We have previously explained this increase as due to co-precipitation or adsorption of these elements from the surrounding soil solutions onto the freshly-formed alteration products (Frost et al., 1983). Recently Anand and Gilkes (1985) have studied altered ilmenite grains by transmission electron microscopy and have observed minute crystals of gibbsite and clay minerals within the pores of the weathered grains. They have explained the increasing aluminium and silicon contents with increasing Ti/(Ti + Fe) ratio as a consequence of an increased abundance of pores available for crystallization of clay minerals, as ilmenite and pseudorutile alter isovolumetrically to porous rutile. Whereas our model considers the impurities to be incorporated at the time of leaching and reprecipitation, Anand and Gilkes' model considers the incorporation of impurity elements as an on-going process in the weathering of soils, where the porous leucoxene grains are considered as part of the soil structure. The porous-grain model leads to a simple explanation for the decrease in aluminium-silicon contents at high Ti/(Ti + Fe) ratios, in terms of crystallization and growth of rutile to fill the locally available pore volume, leaving no room for ingress of Al,Si containing soil solutions. Both models probably apply in a groundwater environment.

The interpretation of the minor element distributions in the 0.01–0.10 A magnetic fractions is complicated because of additional alteration mechanisms that operate in the near-surface layers of the heavy mineral deposit and produce strongly magnetic products as discussed above. The oxidation reactions are unlikely to significantly affect the minor element distributions, as the cation diffusions and subsequent phase changes are localized to regions much smaller than the electron beam diameter. However, the direct formation of rutile from ilmenite is expected to have a strong influence on all three minor element distributions. First, since the density change accompanying the ilmenite-to-rutile reaction is considerably greater than that for pseudorutile to rutile, the resulting pore structure is expected to be coarser, leading to the possibility of more ready access of Al- and Si-containing soil solutions to the interior of the grains and consequently higher levels of crystallization of clay minerals within the grains. Second, the direct leaching of ilmenite will dissolve manganese, and where mixtures of the resulting Mn-depleted rutile leach product and unattacked ilmenite are intergrown on a scale finer than the electron beam spread, the Ti/(Ti + Fe) ratio determined from microprobe analyses can lie anywhere between the values for ilmenite and rutile, depending on the proportions of the two phases. Thus for the most-magnetic fractions, reduced manganese concentrations will be associated with the full range of Ti/(Ti +

Fe) ratios, rather than just for $Ti/(Ti + Fe) < 0.7$, as in the ilmenite-pseudorutile-rutile assemblages. Similarly, increased aluminium and silicon concentrations will extend into the composition range with $Ti/(Ti + Fe) < 0.7$. These predicted trends are borne out by the experimental results, as illustrated in Figure 4. The levels of aluminium and manganese in the 0.01 A magnetic fraction are higher and lower, respectively, than those in the 0.3 A fraction over the full composition range.

## References

Anand, R. R. and Gilkes, R. J. (1985) Some alumina and silica in weathered ilmenite grains are present in clay minerals—a response to Frost et al. (1983). Mineralogical Magazine, 49, 141–145.

Baxter, J. L. (1977) Heavy mineral sand deposits of Western Australia. Geological Survey of Western Australia, Mineral Resources Bulletin 10.

Chung, P. H. (1974) Quantitative interpretation of X-ray diffraction patterns of mixtures 1. Matrix flushing method for quantitative multicomponent analysis. Journal of Applied Crystallography, 7, 519–525.

Dimanche, F. and Bartholomé, P. (1976) The alteration of ilmenite in sediments. Minerals Science and Engineering, 8, 187–200.

Flinter, B. H. (1959) The alteration of Malayan ilmenite grains and the question of "arizonite." Economic Geology, 54, 720–729.

Frost, M. T. (1977) A new interactive computer program to process electron microprobe data. Mineralogical Magazine, 41, 414–416.

Frost, M. T., Grey, I. E., Harrowfield, I. R., and Mason, K. (1983) The dependance of alumina and silica contents on the extent of alteration of weathered ilmenites from Western Australia. Mineralogical Magazine, 47, 201–208.

Gevorkyan, V. Kh. and Tananayev, N. V. (1964) Some data on the initial stages of leucoxenization of ilmenite from the sedimentary deposits of the northern Azov area. Dopovidi Adakemii Nauk Ukrains 'Koi RSR, 10, 1366–1369.

Grey, I. E. and Reid, A. F. (1972) Shear structure compounds $(Cr,Fe)_2Ti_{n-2}O_{2n-1}$ derived from the $\alpha$-$PbO_2$ structural type. Journal of Solid State Chemistry, 4, 186–194.

Grey, I. E. and Reid, A. F. (1975) The structure of pseudorutile and its role in the natural alteration of ilmenite. American Mineralogist, 60, 898–906.

Grey, I. E., Reid, A. F., and Allpress, J. G. (1973) Compounds in the system $Cr_2O_3$–$Fe_2O_3$–$TiO_2$–$ZrO_2$ based on intergrowth of the $\alpha$-$PbO_2$ and $V_3O_5$ structural types. Journal of Solid State Chemistry, 8, 86–99.

Grey, I. E., Li, C., and Watts, J. A. (1983) Hydrothermal synthesis of goethite-rutile intergrowth structures and their relationship to pseudorutile. American Mineralogist, 68, 981–988.

Haggerty, S. E. (1976) Oxidation of opaque mineral oxides in basalts. In D. Rumble III, Ed., Oxide Minerals, Reviews in Mineralogy, Volume 3, Hg-28. Mineralogical Society of America, Washington, D.C.

Larrett, M. J. W. and Spencer, W. G. (1971) Contributions to Australasian mineralogy 3 'pseudorutile' from South Neptune Island, South Australia. Amdel Bulletin, 12, 74–80.

Lindsley, D. H (1965) Iron-titanium oxides. Carnegie Institution Washington Year Book, 64, 144–148.

Lynd, L. E. (1960) Study of the mechanism and rate of ilmenite weathering. AIME Transactions, 217, 311–318.

Rao, D. B. and Rigaud, M. (1974) Oxidation of ilmenite and the product morphology. High Temperature Science, 6, 323–341.

Rumble, D. (1976) Oxide minerals in metamorphic rocks. In D. Rumble III, Ed., Oxide Minerals, Reviews in Mineralogy, Volume 3, R-3. Mineralogical Society of America, Washington, D.C.

Temple, A. K. (1966) Alteration of ilmenite. Economic Geology, 61, 695–714.

Wort, M. J. and Jones, M. P. (1980) X-ray diffraction and magnetic studies of altered ilmenite and pseudorutile. Mineralogical Magazine, 43, 659–663.

Wort, M. J. and Jones, M. P. (1981) Magnetic properties of ilmenite, detrital altered ilmenite and pseudorutile. Transactions of Institution of Mining and Metallurgy (Sect. C: Mineral Processing and Extractive Metallurgy), 90, C130–137.